ORCA – Online Research @ Cardiff

Supramolecular Assembly of Molecular Rare-Earth−3,5-Dichlorobenzoic Acid−2,2′:6′,2″-Terpyridine Materials: Structural Systematics, Luminescence Properties, and Magnetic Behavior

Korey P. Carter,[†] Kara E. Thomas,[†] Simon J. A. Pope,[‡] Rebecca J. Holmberg,[§] Ray J. Butcher,[‖] Muralee Murugesu,[§] and Christopher L. Cahill*,[†]

[†]Department of Chemistry, The George Washington University, 800 22nd Street, Northwest, Washington, D.C. 20052, United States
[‡]School of Chemistry, Cardiff University, Main Building, Cardiff, Cymru/Wales CF10 3AT, U.K.
[§]Department of Chemistry and Biomolecular Sciences, University of Ottawa, 10 Marie Curie, Ottawa, ON, Canada K1N 6N5
[‖]Department of Chemistry, Howard University, 525 College Street, Northwest, Washington, D.C. 20059, United States

Ⓢ *Supporting Information*

ABSTRACT: The syntheses and crystal structures of 16 new rare-earth (RE = La^{3+}−Y^{3+})−3,5-dichlorobenzoic acid−terpyridine molecular materials characterized via single-crystal and powder X-ray diffraction are reported. These 16 complexes consist of four unique structure types ranging from molecular dimers (La^{3+} and Ce^{3+}) to tetramers (Pr^{3+}−Y^{3+}) as one moves across the RE^{3+} series. This structural evolution is accompanied by subsequent changes in modes of supramolecular assembly (halogen bonding, halogen−π, halogen−halogen, and π−π interactions). Solid-state visible and near-infrared lifetime measurements were performed on complexes **6** (Sm^{3+}), **7** (Eu^{3+}), **9** (Tb^{3+}), **10** (Dy^{3+}), **11** (Ho^{3+}), **12** (Er^{3+}), and **14** (Yb^{3+}), and characteristic emission was observed for all complexes except **11**. Lifetime data for **11**, **12**, and **14** suggest sensitization by the terpy antenna does occur in near-infrared systems, although not as efficiently as in the visible region. Additionally, direct current magnetic susceptibility measurements were taken for complexes **10** (Dy^{3+}) and **12** (Er^{3+}) and showed dominant ferromagnetic behavior.
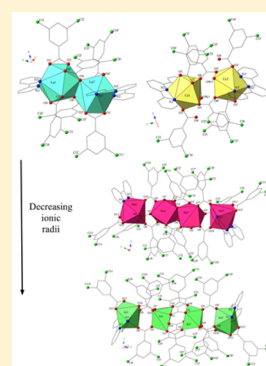
INTRODUCTION

The coordination chemistry of molecular rare-earth materials has been studied rather extensively,[1−7] yet these materials continue to be a topic of fundamental interest because of the diverse nature of applications for which these materials have shown promise, including luminescent bioprobes,[8,9] electroluminescent materials,[10,11] nonlinear optics,[12,13] and single-molecule magnets (SMMs).[14−17] These applications are made possible by the characteristic luminescent and magnetic behavior of the rare-earth elements, which stem from the shielding of 4f orbitals by 5s and 5p orbitals and the large numbers of unpaired electrons of each RE^{3+} metal center.[18] Efficient utilization of the unique luminescent properties of RE^{3+} metal centers often relies on sensitization via organic chromophores with triplet-state energies in the appropriate range for energy transfer,[2,19] whereas taking advantage of the spin−orbit interactions and single-ion anisotropy of RE^{3+} ions to probe single-molecule magnetic behavior (SMM) requires the precise orientation of the anisotropic axes of both the ligands and the RE^{3+} cations.[20,21] The ligands used herein were selected with these criteria in mind to explore whether we could efficiently sensitize RE^{3+} cations while also observing SMM behavior.

Harnessing the unique capabilities of rare-earth metal cations so that one may selectively tune the resulting properties involves exercising some level of control over the first coordination sphere of the RE^{3+} ions, and this remains a challenge in rare-earth hybrid

material synthesis.[1,6,7] One route that allows for a modest degree of control over coordination geometry and ultimately over extended solid-state structures is a dual-ligand strategy in which a chelating N-donor "caps" the RE^{3+} metal center and functionalized benzoic acid ligands then complete the RE^{3+} first coordination environment, subsequently "linking" the RE^{3+} ions into discrete mono- or polynuclear units. It is this approach that we have utilized herein, and vital to this approach is the formation of a molecular RE^{3+} complex (or "tecton"), which will then be assembled through chemically robust, attractive motifs ("synthons") made possible by the various functional groups at the complex's periphery.

The synthesis of molecular rare-earth materials based on such a combination of coordination and supramolecular chemistry principles is a topic of continued interest in our lab, and we have demonstrated the utility of this strategy in both molecular and extended structures.[22−24] Essential to this strategy is the use of a capping ligand, to control and restrict the geometry of the RE^{3+} first coordination sphere, and herein, we utilize the tridentate N-donor 2,2′:6′,2″-terpyridine (terpy), a versatile starting material for inorganic and supramolecular synthesis.[5,25] The inclusion of terpy allows for the promotion of a single polynuclear tecton and assembly thereof via supramolecular synthons at the

periphery of the "linker" ligand. For this study, the choice of 3,5-dichlorobenzoic as a linker was made with the explicit intent of exploring halogen bonding in molecular rare-earth systems, a topic we have investigated only implicitly in our previous efforts.[22,23]

Building on our previous work exploring supramolecular assembly in both 4f and 5f systems,[22−24,26,27] we herein report the synthesis, crystal structures, visible and near-infrared (near-IR) luminescent properties, and magnetic behavior (for the Dy[3+] and Er[3+] species) for a family of 16 molecular rare-earth materials featuring both 3,5-dichlorobenzoic acid and terpy. The dimeric and tetrameric tectons each feature a fixed local geometry in which supramolecular synthons [halogen−halogen, halogen bonding (X···O), halogen−π, or π−π] at the periphery of the RE[3+] coordination sphere link the molecular tectons into extended two- and three-dimensional topologies. Moreover, this systematic study of molecular rare-earth materials that incorporate both 3,5-dichlorobenzoic acid and terpy highlights the variation in observed supramolecular synthons that may be correlated to the nuclearity and the nature of the local geometry of the first coordination sphere, as well as to the lanthanide contraction.

■ EXPERIMENTAL SECTION

Materials and Methods. La(NO$_3$)$_3$·6H$_2$O (Strem Chemicals, 99.9%), LaCl$_3$ (Alfa Aesar, 99.9%), Ce(NO$_3$)$_3$·6H$_2$O (Sigma-Aldrich, 99%), Sm(NO$_3$)$_3$·6H$_2$O (Alfa Aesar, 99.9%), Ln(NO$_3$)$_3$·xH$_2$O (where Ln = Pr[3+], Eu^{3+}, Gd^{3+}, Tb[3+], Dy[3+], Ho[3+], Er[3+], Yb[3+], or Y[3+] and x = 1, 5, or 6; Strem Chemicals, 99.9%), Ln(NO$_3$)$_3$·xH$_2$O (where Ln = Nd[3+], Tm[3+], or Lu[3+] and x = 1, 5, or 6; Sigma-Aldrich, 99.9%), 3,5-dichlorobenzoic acid (Alfa Aesar, 99%), and 2,2′:6′,2″-terpyridine (Alfa Aesar, 97%) were used for syntheses as received.

Synthesis. Complexes 1−16 were synthesized via hydrothermal methods in a 23 mL Teflon-lined autoclave at an oven temperature of 150 °C. A mixture of LaCl$_3$ (1) or Ln[3+] nitrate hydrate [Ln(NO$_3$)$_3$·xH$_2$O, where Ln = La−Y and x = 1, 5, or 6] (2−16), 3,5-dichlorobenzoic acid (C$_7$H$_3$Cl$_2$O$_2$), 2,2′:6′,2″-terpyridine (C$_{15}$H$_{11}$N$_3$), and distilled water (molar ratio of 1:2:1:826) was heated for 72 h. Autoclaves were allowed to cool to room temperature over 4 h and then opened after approximately 12 h. Colorless or pink, in the case of Ho[3+] and Er[3+], small, block crystals were obtained from the bulk product after decanting the supernatant liquor, washing three times with distilled water and ethanol, and air-drying at room temperature overnight. A further comment regarding 1 and 2 is that the latter can also be synthesized by starting with LaCl$_3$ using the procedure described above if the water concentration is doubled (from 1.5 to 3 mL).

Characterization. *X-ray Structure Determination.* Single crystals from each bulk sample were isolated and mounted on MiTeGen micromounts. Structure determination for each of the single crystals was achieved by collecting reflections using 0.5° ω scans on a Bruker SMART diffractometer furnished with an APEX II CCD detector using Mo Kα (λ = 0.71073 Å) radiation at a low temperature (100 K). Integration was done using the *SAINT* software package[28] that is a part of the APEX II software suite,[29] and absorption corrections were performed using *SADABS*.[30] Nonmerohedral twinning in crystals of complexes 8 and 10 (two components) was accounted for using *TWINABS*.[31] Structures of complexes 1−8, 11, and 13−16 were determined via direct methods using *SIR 92*,[32] whereas structures of complexes 9, 10, and 12 were determined via the Patterson method (*SHELXS-2014*).[33] All 16 complexes were refined using *SHELXL-2014*[33] in the *WinGX*[34] software suite. In each structure, all non-hydrogen atoms were located via difference Fourier maps and refined anisotropically. Aromatic hydrogen atoms were placed at their idealized positions by employing the HFIX43 instruction and allowed to ride on the coordinates of their parent carbon atom (U$_{iso}$ fixed at 1.2U$_{eq}$). Hydrogen atoms on bound water molecules in complexes 2 and 3 were located and modeled with DFIX restraints. Positional disorder in 2,2′:6′,2″-terpyridine ligands in complexes 1 (C14) and 6 (C55) was restrained via the ISOR command with uncertainty values (based on the extent of the disorder) of 0.001 and 0.01 used in the refinements of 1 and 6, respectively. Complexes 4 and 5 lie at the transition point between dimers and tetramers in this family of materials, and perhaps as a consequence, these two materials feature significant disorder. In 4 and 5, split chlorine atoms were accounted for via the PART and EADP commands. Whole molecule disorder of the terpy moieties in both materials was modeled via the PART, AFIX, EADP, and ISOR commands where necessary. Further, both 4 and 5 feature a disordered water molecule that is coordinated to one of the two crystallographically unique Pr[3+] and Nd[3+] metal centers (Pr1 and Nd1), which was modeled as half-occupancy for 4 and one-quarter occupancy for 5. All figures were prepared with CrystalMaker.[35] Data collection and refinement details for complexes 1−16 are included in Table 1.

Powder X-ray Diffraction. Powder X-ray diffraction (PXRD) data on the bulk reaction product of complexes 1−16 (Figures S8−S23) were used to examine the bulk purity of each sample. All data were collected on a Rigaku Miniflex (Cu Kα; 2θ = 3−60°) and analyzed using the JADE software program.[36] The bulk products of 1, 4, and 5 are biphasic, and the impurities in each sample were successfully identified (Figures S8, S11, and S12). Complex 1 coforms with 2 (structure types I and II), whereas the impurities in 4 and 5 (structure type III) are the Pr[3+] and Nd[3+] analogues of complex 3 (structure type II). These findings suggest that these two structure types, I and II (for La^{3+}), and II and III (for Pr[3+] and Nd[3+]), may be close in stability and are thus capable of accommodating more than one specific RE[3+] metal center.

Luminescence Measurements. Room-temperature solid-state visible luminescence measurements were obtained for 6, 7, 9, and 10 on a Horiba JobinYvon Fluorolog-3 spectrophotometer. Near-IR photo-physical data for 12 and 14 were obtained on a Horiba JobinYvon Fluorolog-3 spectrometer fitted with a Hamamatsu R5509-73 detector (cooled to −77 °C using C9940 housing). All data were collected and manipulated using the FluoroEssence software package, and final plots of the solid-state spectra were made in Microsoft Excel.

Lifetime data were collected for 6, 7, 9−12, and 14 on a Horiba JobinYvon Fluorolog-3 spectrometer fitted with a JY TBX picosecond photodetection module and a Continuum Minilite Nd:YAG pulsed laser configured for 355 nm output. Lifetime profiles for all seven complexes were obtained using the JobinYvon FluoroHub single-photon counting module, and the data were fit using the DAS6 software.

Magnetic Measurements. Magnetic measurements were performed using a Quantum Design SQUID magnetometer (MPMS-XL7), operating between 1.8 and 300 K for dc-applied fields ranging from −7 to 7 T. Susceptibility measurements were performed on powder samples of 26.9 mg of complex 10 (Dy[3+]) and 31.2 mg of complex 12 (Er[3+]), each wrapped within a polyethylene membrane. Direct current (dc) susceptibility measurements were taken at 1000 Oe. The magnetization data were initially collected at 100 K to check for ferromagnetic impurities, found to be absent in all samples.

■ RESULTS

Description of Structures. Single-crystal X-ray crystallography analyses yielded four unique structure types in this series of molecular complexes as detailed in Table 2. Structure types I and II can be described as binuclear species, whereas structure types III and IV can be described as tetranuclear species; a representative structural example (1, 3, 6, and 12) will be presented in detail.

[La(C$_{15}$H$_{11}$N$_3$)(C$_7$H$_3$Cl$_2$O$_2$)$_3$]$_2$ (1), with Structure Type I. Complex 1 crystallizes in space group $P\bar{1}$ and features a single crystallographically unique La^{3+} ion with a coordination number of 10. The La^{3+} center displays a bicapped square antiprismatic molecular geometry and is bound by a tridentate terpy and three 3,5-dichlorobenzoic acid ligands adopting either the chelating−bridging bidentate or bidentate coordination mode (Figure 1). La1−O bond distances for the chelating−bridging bidentate 3,5-dichlorobenzoic acid are 2.536(2) Å (La1−O5), 2.5734(19) Å (La1−O6), and 2.760(2) Å (La1′−O6), and La1−O bond

Table 1. Crystallographic Data for Complexes 1−16 (structure types I−IV)

	1 (I)	2 (II)	3 (II)	4 (III)
chemical formula	$C_{72}H_{40}Cl_{12}N_6O_{12}La_2$	$C_{72}H_{44}Cl_{12}N_6O_{14}La_2$	$C_{72}H_{44}Cl_{12}N_6O_{14}Ce_2$	$C_{114}H_{60}Cl_{24}N_6O_{25}Pr_4$
formula weight	1884.32	1920.35	1922.77	3328.12
crystal system	triclinic	triclinic	triclinic	triclinic
space group	$P\bar{1}$	$P\bar{1}$	$P\bar{1}$	$P\bar{1}$
a (Å)	12.3170(10)	10.5927(10)	10.6010(8)	12.8210(7)
b (Å)	12.3233(10)	13.1980(12)	13.2245(10)	16.1881(8)
c (Å)	14.1422(12)	15.4800(14)	15.4213(12)	16.7008(9)
α (deg)	67.844(10)	67.675(11)	67.719(8)	75.310(3)
β (deg)	73.242(11)	88.912(12)	88.784(9)	69.026(3)
γ (deg)	67.030(10)	69.615(12)	69.386(9)	79.672(4)
V (Å^3)	1805.2(3)	1860.5(4)	1856.7(3)	3115.7(3)
Z	1	1	1	1
T (K)	100(2)	100(2)	100(2)	100(2)
λ (Mo Kα)	0.71073	0.71073	0.71073	0.71073
D_{calc} (g cm^{-3})	1.733	1.714	1.720	1.774
μ (mm^{-1})	1.678	1.632	1.711	2.123
R_{int}	0.0492	0.0471	0.0411	0.0448
R1 $[I > 2\sigma(I)]$	0.0332	0.0286	0.0296	0.0350
wR2 $[I > 2\sigma(I)]$	0.0632	0.0612	0.0608	0.0745
	5 (III)	**6 (III)**	**7 (III)**	**8 (III)**
chemical formula	$C_{114}H_{59}Cl_{24}N_6O_{24.5}Nd_4$	$C_{114}H_{58}Cl_{24}N_6O_{24}Sm_4$	$C_{114}H_{58}Cl_{24}N_6O_{24}Eu_4$	$C_{114}H_{58}Cl_{24}N_6O_{24}Gd_4$
formula weight	3332.43	3347.86	3354.30	3375.46
crystal system	triclinic	triclinic	triclinic	triclinic
space group	$P\bar{1}$	$P\bar{1}$	$P\bar{1}$	$P\bar{1}$
a (Å)	12.8146(10)	12.7959(6)	12.7973(7)	12.762(6)
b (Å)	16.1805(12)	16.2074(7)	16.2106(9)	16.214(7)
c (Å)	16.6822(13)	16.6533(7)	16.6378(9)	16.564(7)
α (deg)	75.230(11)	74.992(4)	74.907(1)	74.969(4)
β (deg)	68.990(11)	68.870(3)	68.772(2)	68.961(5)
γ (deg)	79.714(12)	79.511(4)	79.499(1)	79.614(5)
V (Å^3)	3107.8(5)	3096.5(3)	3091.5(3)	3075.0(2)
Z	1	1	1	1
T (K)	100(2)	100(2)	100(2)	100(2)
λ (Mo Kα)	0.71073	0.71073	0.71073	0.71073
D_{calc} (g cm^{-3})	1.781	1.795	1.802	1.823
μ (mm^{-1})	2.231	2.458	2.592	2.722
R_{int}	0.0286	0.0383	0.0370	0.0539
R1 $[I > 2\sigma(I)]$	0.0266	0.0310	0.0306	0.0388
wR2 $[I > 2\sigma(I)]$	0.0617	0.0692	0.0612	0.0949
	9 (III)	**10 (IV)**	**11 (IV)**	**12 (IV)**
chemical formula	$C_{114}H_{58}Cl_{24}N_6O_{24}Tb_4$	$C_{114}H_{58}Cl_{24}N_6O_{24}Dy_4$	$C_{114}H_{58}Cl_{24}N_6O_{24}Ho_4$	$C_{114}H_{58}Cl_{24}N_6O_{24}Er_4$
formula weight	3382.14	3396.46	3406.18	3415.50
crystal system	triclinic	triclinic	triclinic	triclinic
space group	$P\bar{1}$	$P\bar{1}$	$P\bar{1}$	$P\bar{1}$
a (Å)	12.7734(8)	12.7502(13)	12.7560(9)	12.7484(15)
b (Å)	16.2509(10)	16.3218(16)	16.3167(11)	16.3141(19)
c (Å)	16.5612(10)	16.4396(16)	16.4387(11)	16.4296(19)
α (deg)	74.915(3)	74.909(7)	74.929(10)	74.927(8)
β (deg)	68.995(3)	79.710(8)	79.748(11)	79.759(9)
γ (deg)	79.546(4)	70.042(8)	70.023(9)	70.013(9)
V (Å^3)	3083.9(3)	3089.6(6)	3090.0(4)	3085.8(7)
Z	1	1	1	1
T (K)	100(2)	100(2)	100(2)	100(2)
λ (Mo Kα)	0.71073	0.71073	0.71073	0.71073
D_{calc} (g cm^{-3})	1.821	1.825	1.830	1.838
μ (mm^{-1})	2.857	2.982	3.124	3.283
R_{int}	0.0464	0.0397	0.0557	0.0325
R1 $[I > 2\sigma(I)]$	0.0414	0.0269	0.0331	0.0239
wR2 $[I > 2\sigma(I)]$	0.0993	0.0575	0.0654	0.0546

Table 1. continued

	13 (IV)	14 (IV)	15 (IV)	16 (IV)
chemical formula	$C_{114}H_{58}Cl_{24}N_6O_{24}Tm_4$	$C_{114}H_{58}Cl_{24}N_6O_{24}Yb_4$	$C_{114}H_{58}Cl_{24}N_6O_{24}Lu_4$	$C_{114}H_{58}Cl_{24}N_6O_{24}Y_4$
formula weight	3422.18	3438.62	3446.34	3102.10
crystal system	triclinic	triclinic	triclinic	triclinic
space group	$P\bar{1}$	$P\bar{1}$	$P\bar{1}$	$P\bar{1}$
a (Å)	12.7386(8)	12.7384(9)	12.7351(7)	12.7564(8)
b (Å)	16.3002(10)	16.2786(11)	16.2643(10)	16.3271(11)
c (Å)	16.4211(10)	16.4168(11)	16.3930(11)	16.4585(11)
α (deg)	74.889(11)	74.792(6)	74.891(10)	74.881(9)
β (deg)	79.660(11)	79.742(7)	79.835(10)	79.538(10)
γ (deg)	69.959(10)	69.923(7)	69.948(11)	70.008(9)
V (Å³)	3077.2(4)	3070.8(4)	3065.1(4)	3093.7(4)
Z	1	1	1	1
T (K)	100(2)	100(2)	100(2)	100(2)
λ (Mo Kα)	0.71073	0.71073	0.71073	0.71073
D_{calc} (g cm⁻³)	1.847	1.859	1.867	1.665
μ (mm⁻¹)	3.449	3.612	3.788	2.447
R_{int}	0.0304	0.0413	0.0319	0.0541
R1 $[I > 2\sigma(I)]$	0.0228	0.0275	0.0219	0.0395
wR2 $[I > 2\sigma(I)]$	0.0513	0.0595	0.0488	0.0864

Table 2. Structural Breakdown of RE³⁺−35diClBA−TPY (1−16) Structure Types I−IV[a]

La³⁺	Ce³⁺	Pr³⁺	Nd³⁺	Pm³⁺	Sm³⁺	Eu³⁺	Gd³⁺	Tb³⁺	Dy³⁺	Ho³⁺	Er³⁺	Tm³⁺	Yb³⁺	Lu³⁺	Y³⁺
II, I	II	III, II	III, II		III	III	III	IV	IV	IV	IV	IV	IV	IV	IV

[a]In split cells, the major structure type is listed first with the minor phase listed second.
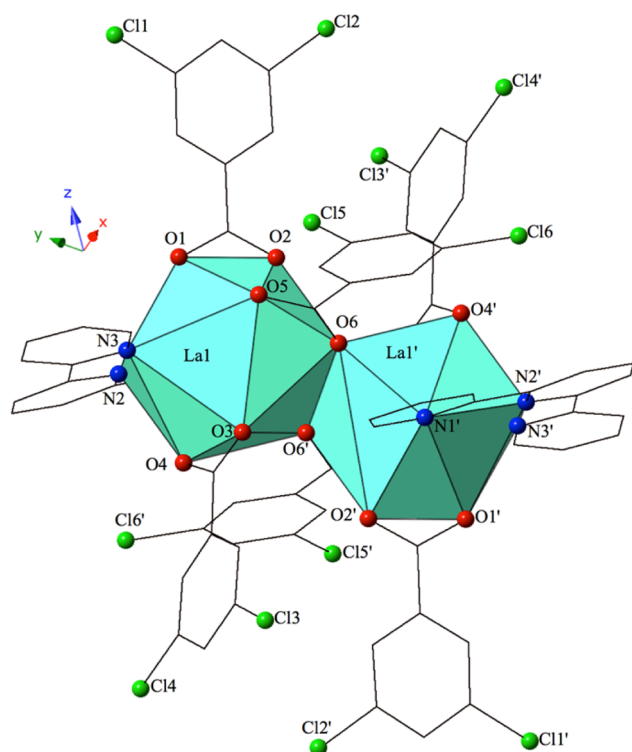
Figure 1. Polyhedral representation of complex **1** (structure type I). Teal polyhedra are La³⁺ metal centers; green, blue, and red spheres represent chlorine, nitrogen, and oxygen atoms, respectively. All H atoms have been omitted for the sake of clarity.

distances to the bidentate 3,5-dichlorobenzoic acid groups (O1−O4) are at an average La−O distance of 2.597 Å. Completing the first coordination sphere of **1** is the tridentate terpy ligand (N1−N3), and the average La−N distance is 2.686 Å. La1 bridges

to a second, symmetry equivalent, La³⁺ metal center (La1′) via edge sharing through carboxylate O6 to form a dimer, or binuclear tecton.

The binuclear tectons of **1** are assembled into a supramolecular one-dimensional (1D) chain along the [001] direction via type I halogen−halogen (Cl4−Cl4) interactions, as defined by Desiraju and colleagues,[37,38] between 3,5-dichlorobenzoic acid ligands on neighboring units (Figure 2). The Cl4−Cl4 distance is 3.0635(18) Å, representing 87.5% of the sum of the van der Waals radii, with corresponding θ_1 and θ_2 angles ($\angle$C−Cl···Cl) of 158.95(16)°. The tectons of **1** are further linked to form a supramolecular two-dimensional (2D) sheet in approximately the (110) plane via localized Cl−π (Cl1−C29) interactions[39] between 3,5-dichlorobenzoic acid ligands on neighboring units, one of which is also participating in the halogen−halogen interaction described above (Figure 2). Halogen−π interaction strengths have been defined previously[40] and are based on how intermolecular interaction distances compare to the corresponding sum of the van der Waals radii (3.450 Å for chlorine and carbon). The interactions between the chlorine (Cl1) of one 3,5-dichlorobenzoic acid a carbon atom from the benzene ring of a 3,5-dichlorobenzoic acid ligand (C29) on the neighboring unit are at a distance of 3.350(3) Å, (97.1% sum of the van der Waals radii) which is indicative of a strong Cl−π interaction.

[Ln($C_{15}H_{11}N_3$)($C_7H_3Cl_2O_2$)₃(H_2O)]₂ (where Ln = La³⁺ and Ce³⁺) (2 and 3, respectively), with Structure Type II. Complexes **2** and **3** are isomorphous, and therefore, only the Ce³⁺ complex (**3**) will be described in detail. Complex **3** features a single crystallographically unique Ce³⁺ metal center with a coordination number of 9, and the molecular geometry around the Ce1 is best described as distorted square antiprismatic. Ce1 is bound by a tridentate terpy, a bound water molecule, and three 3,5-dichlorobenzoic acid ligands each adopting a different co-ordination mode: bridging bidentate, bidentate, or monodentate
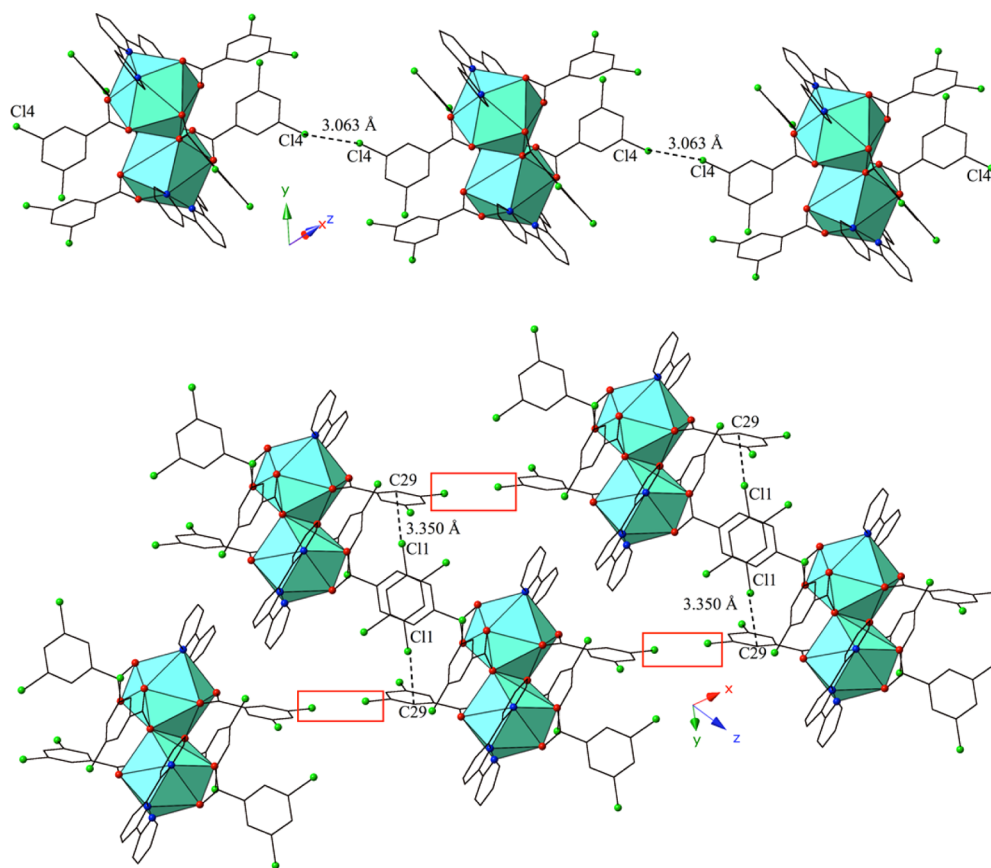
Figure 2. Complex **1** viewed along approximately the [001] direction (top) featuring a type I Cl−Cl interaction that links adjacent La^{3+} tectons. **1** viewed in approximately the (110) plane (bottom) illustrating the localized Cl−π interactions that further assemble La^{3+} tectons into a supramolecular 2D sheet. Type I Cl−Cl interactions that link tectons of **1** into the 1D chain are highlighted by red boxes.

(Figure 3). Ce1−O bond distances for the bidentate 3,5-dichlorobenzoic acid group (O1 and O2) are 2.6163(17) and 2.5688(17) Å, respectively, and for the bridging bidentate 3,5-dichlorobenzoic acid group are 2.4813(17) Å (Ce1−O5) and 2.4584(17) Å (Ce1−O6). A monodentate 3,5-dichlorobenzoic acid ligand (O3) is also coordinated to the Ce^{3+} metal center at a bond distance of 2.4544(17) Å, and the coordinated water molecule, OW1, has a Ce1−OW1 bond distance of 2.4872(18) Å. Completing the coordination sphere of the Ce^{3+} metal center is a tridentate terpy molecule (N1−N3), and the average Ce1−N distance is 2.700 Å. Ce1 is linked to a second, symmetry equivalent, Ce^{3+} metal center (Ce1′) to form a binuclear tecton similar to **1**, via carboxylate O5 and O6 atoms from a bridging bidentate 3,5-dichlorobenzoic acid ligand.

The binuclear tectons of **3** are assembled via a bifurcated halogen−halogen interaction (Cl1−Cl1 and Cl1−Cl3) in which the chlorine atom (Cl1) of one 3,5-dichlorobenzoic acid ligand functions as both a halogen bond donor and acceptor to form a sheet in approximately the (011) plane (Figure 4). The bifurcated interaction consists of a type I interaction between Cl1 atoms on neighboring tectons with a Cl1−Cl1 distance of 3.2217(11) Å (92.0% of the sum of the van der Waals radii) and a type II halogen−halogen interaction (Cl1−Cl3) as defined by Desiraju et al.[38] where the interaction distance is 3.3229(12) Å (94.9% of the sum of the van der Waals radii), and the θ_1 (C26−Cl3−Cl1) and θ_2 (C19−Cl1−Cl3) values are 158.98(12)° and 91.80(11)°, respectively.

Further assembly of the tectons of **3** into a supramolecular three-dimensional (3D) network is the result of halogen bonding
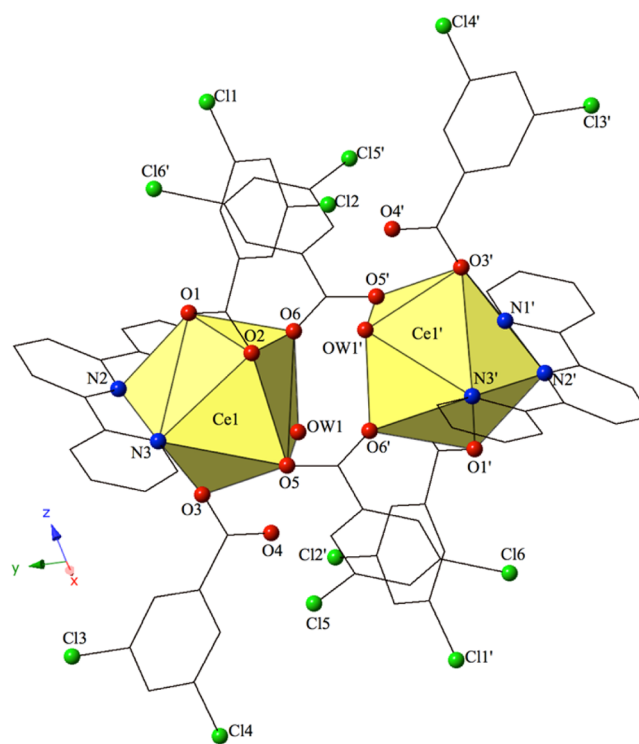
Figure 3. Polyhedral representation of complex **3** (Ce^{3+}) (structure type II). Yellow polyhedra are Ce^{3+} metal centers.
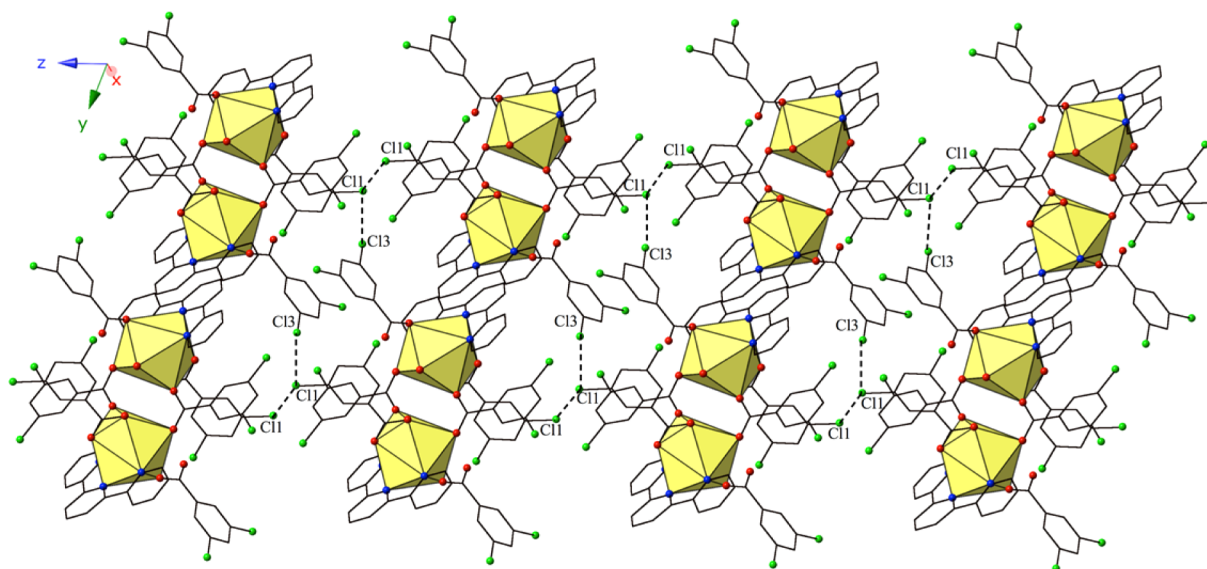
Figure 4. Complex **3** viewed in the (011) plane illustrating the bifurcated halogen−halogen interactions that tether Ce^{3+} tectons to form a 2D sheet.
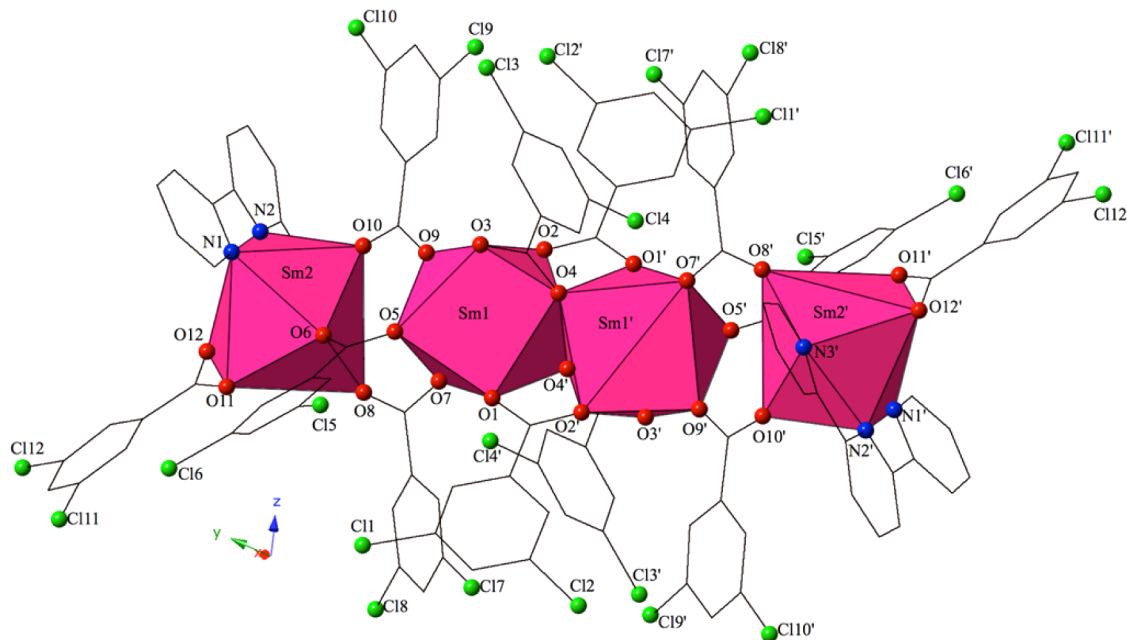

Figure 5. Polyhedral representation of complex **6** (Sm^{3+}) (structure type III). Pink polyhedra are Sm^{3+} metal centers.

(Cl2−O2) and localized Cl−π (Cl2−C15) interactions between a 3,5-dichlorobenzoic acid ligand on one Ce^{3+} unit and a 3,5-dichlorobenzoic acid ligand and a terpy moiety on the neighboring unit (Figure S1). The halogen bonding interactions are between the carboxylate oxygen (O2) and the chlorine from a 3,5-dichlorobenzoic acid ligand (Cl2) on the neighboring Ce^{3+} dimer, and the corresponding Cl−O interaction distance and angle (∠C−Cl−O) are 3.143(2) Å and 142.55(10)°, respectively. The moderately strong[40] localized Cl−π interaction (Cl2−C15) is between the chlorine (Cl2) of one 3,5-dichlorobenzoic acid and a carbon atom (C15) on a neighboring terpy ligand at a distance of 3.431(3) Å (99.4% of the sum of the van der Waals radii).

[Ln$_2$(C$_{15}$H$_{11}$N$_3$)(C$_7$H$_3$Cl$_2$O$_2$)$_6$]$_2$ (where Ln = Pr^{3+}−Tb^{3+}) (4−9, respectively), with Structure Type III. Complexes **4−9** are isomorphous, and therefore, only the Sm^{3+} complex (**6**) will

be described in detail. The asymmetric unit of **6** contains two crystallographically unique Sm^{3+} ions that each have a coordination number of 8 and adopt molecular geometries that can be described as square antiprismatic (Sm1) and bicapped trigonal prismatic (Sm2), respectively (Figure 5). Sm1 is bound by five 3,5-dichlorobenzoic acid ligands, which adopt either the chelating−bridging bidentate or bridging bidentate coordination mode through the oxygen atoms (O1−O4, O4′, O5, O7, and O9) at an average Sm−O distance of 2.148 Å. Sm2 is chelated by a tridentate terpy molecule and then further bound to four 3,5-dichlorobenzoic acid ligands adopting either the bidentate or bridging bidentate coordination mode. Sm−O bond distances to Sm2 are on average 2.396 Å in length, whereas Sm−N bond distances to the terpy moiety (bound through N1−N3) are on average 2.570 Å in length.

The tetranuclear tectons of **6** are linked to form a 2D sheet in approximately the (011) plane via a pair of halogen−halogen
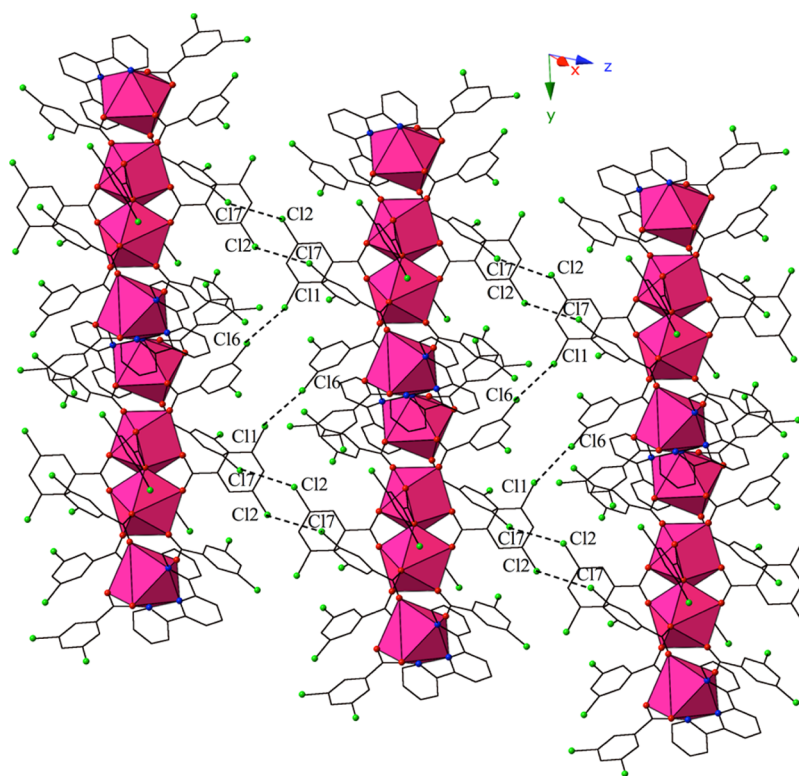
Figure 6. Complex **6** viewed in the (011) plane illustrating the pair of halogen−halogen interactions that link tetranuclear Sm³⁺ tectons to form a supramolecular 2D sheet.

interactions (Cl1−Cl6 and Cl2−Cl7) in which the chlorine atoms (Cl1 and Cl2) of one 3,5-dichlorobenzoic acid ligand interact with chlorine atoms (Cl6 and Cl7) from 3,5-dichlorobenzoic acid ligands on two neighboring units (Figure 6). The two interactions adopt geometries that can be described as quasi-type I and type I[38] and have lengths of 3.2623(14) Å (Cl1−Cl6) and 3.4016(19) Å (Cl2−Cl7), respectively. Corresponding angles (∠C−Cl···Cl) for the interactions are 150.57(15)° and 130.02(14)° (quasi-type I Cl1−Cl6 interaction) and 139.55(17)° and 138.83(12)° (type I Cl2−Cl7 interaction).

Supplementing the assembly of **6** into layers is a bifurcated halogen−halogen interaction (Cl7−Cl8 and Cl8−Cl9) in which a chlorine atom from one 3,5-dichlorobenzoic acid ligand (Cl8) acts as a halogen bond acceptor further linking the tetranuclear units of **6** in approximately the (011) plane (Figure 7). The bifurcated linkage may be described as a combination of a type I interaction[38] between Cl8 (halogen bond acceptor) and a chlorine atom (Cl9) at the 5-position of a 3,5-dichlorobenzoic acid ligand on an adjacent Sm³⁺ unit and a quasi-type I interaction[38] between Cl8 and a chlorine (Cl7) from another 3,5-dichlorobenzoic ligand on the same adjacent unit. The Cl8−Cl9 distance is 3.2710(18) Å [93.5% of the sum of the van der Waals (vdW) radii], and the θ_1 (C32−Cl9−Cl8) and θ_2 (C27−Cl8−Cl9) angles are very near ideal type I geometry ($\theta_1 = \theta_2$) at 163.40(16)° and 155.72(13)°, respectively. The Cl7−Cl8 distance is 3.499(2) Å (99.9% of the sum of vdW radii), and the θ_1 (C27−Cl8−Cl7) and θ_2 (C25−Cl7−Cl8) values are 124.62(13)° and 95.85(12)°, respectively.

Further assembly of **6** into a supramolecular 3D topology is the result of cooperative Cl−O halogen bonding and a fifth Cl−Cl halogen−halogen interaction (Figure S2). The halogen bonding interaction is between the carboxylate O12 of a 3,5-dichlorobenzoic ligand on one unit and the chlorine atom

(Cl5) from a 3,5-dichlorobenzoic acid ligand on a neighboring unit. The corresponding distance and angle for this interaction are 3.127(3) Å and 160.95(12)°, respectively. In addition, a type II[38] halogen−halogen interaction (Cl10−Cl12) further links the tetramers of **6**, and the interaction has a length of 3.4035(10) Å (97.2% of the sum of the vdW radii) with θ_1 (C34−Cl10−Cl12) and θ_2 (C41−Cl12−Cl10) values of 144.79(12)° and 103.98(11)°, respectively (Figure S2).

[Ln₂(C₁₅H₁₁N₃)(C₇H₃Cl₂O₂)₆]₂ (where Ln = Dy³⁺−Y³⁺) (10−16, respectively), with Structure Type IV. Complexes **10−16** are isomorphous, and therefore, only the Er³⁺ complex (**12**) will be described in detail. The asymmetric unit of **12** contains two crystallographically unique Er³⁺ ions, and the local structure is very similar to that of **6**; however, the Er³⁺ metal centers (Er1 and Er2) now have coordination numbers of 7 and 8, respectively (Figure 8). Er1 displays a distorted square pyramidal molecular geometry and is coordinated to seven 3,5-dichlorobenzoic acid ligands, each adopting the bridging bidentate coordination mode at an average distance of 2.279 Å. The coordination geometry of Er2 is nearly identical to that of Sm2 in **6** as it is chelated by a tridentate terpy molecule and then further coordinated to four 3,5-dichlorobenzoic acid ligands. The molecular geometry of Er2 can be described as bicapped trigonal prismatic, and average Er2−O and Er2−N bond distances are 2.325 and 2.510 Å, respectively.

The tetranuclear tectons of **12** are linked to form chains that run along [100] via a pair of halogen bonding interactions (Cl1−Cl3 and Cl7−O12). The type II[38] halogen−halogen interaction is between chlorine atoms (Cl1 and Cl3) of 3,5-dichlorobenzoic acid ligands on neighboring units where the Cl1−Cl3 distance is 3.4119(15) Å (97.5% of the sum of the vdW radii) and the θ_1 (C11−Cl3−Cl1) and θ_2 (C4−Cl1−Cl3) values are 168.30(12)° and 111.25(11)°, respectively (Figure 9).
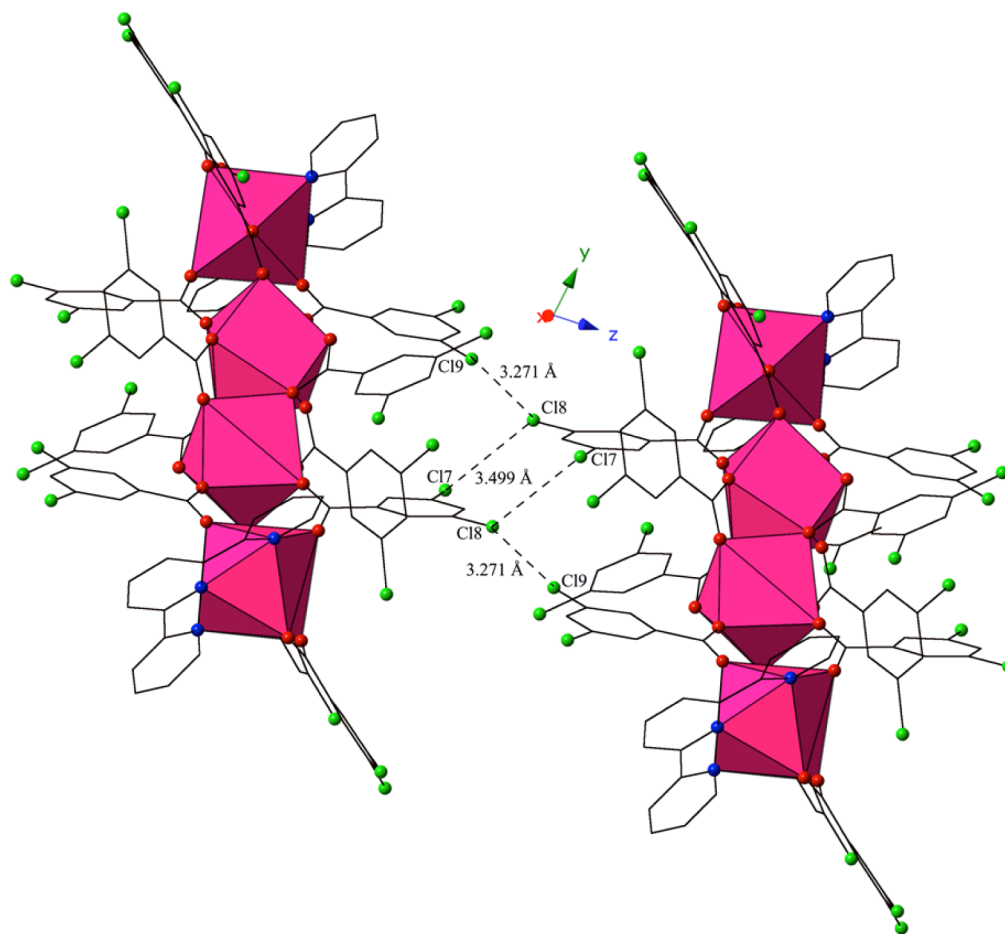
Figure 7. Complex **6** in the (011) plane. The bifurcated halogen−halogen interaction that tethers neighboring Sm^{3+} tetramers is highlighted.
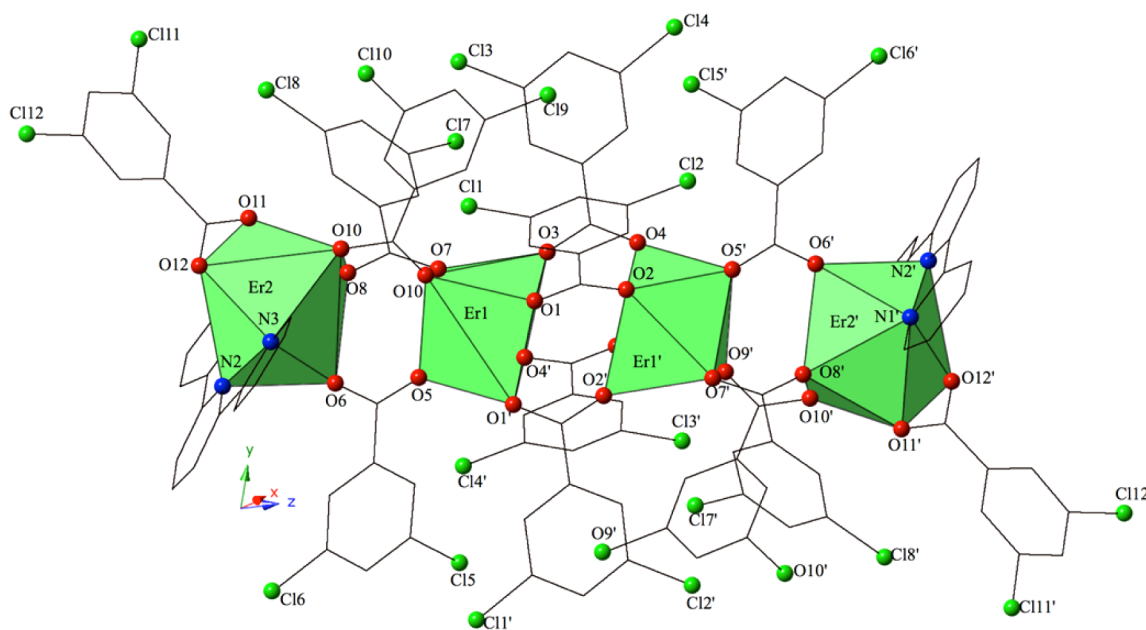
Figure 8. Polyhedral representation of complex **12** (Er^{3+}) (structure type IV). Green polyhedra are Er^{3+} metal centers.

This halogen−halogen interaction is complemented by a halogen bonding interaction (Cl7−O12) between the carboxylate oxygen (O12) and a chlorine from a 3,5-dichlorobenzoic acid ligand (Cl7) on the neighboring Er^{3+} tetramer, and the

corresponding Cl−O interaction distance and angle ($\angle C−Cl−O$) are 3.055(2) Å and 163.21(10)°, respectively.

Assembly of the tectons of **12** into supramolecular 2D sheets is the consequence of a pair of halogen−halogen interactions coupled
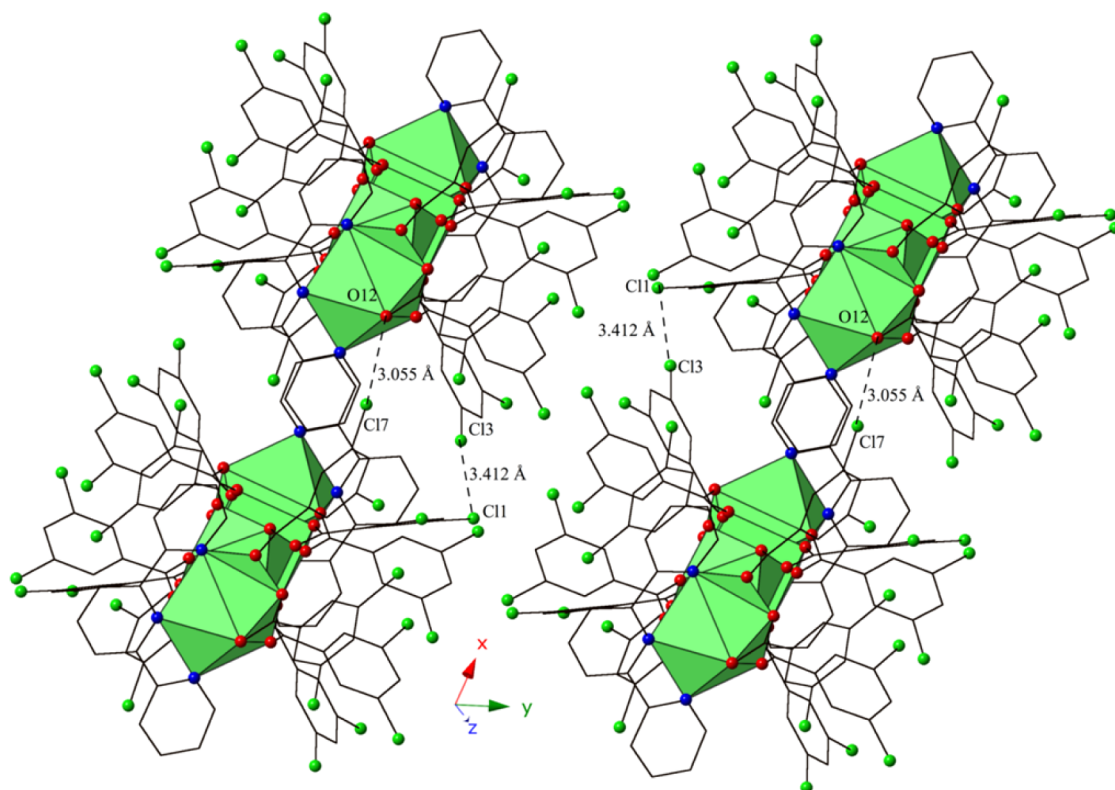
Figure 9. Complex **12** viewed along the [100] direction highlighting the supramolecular interactions that assemble tetranuclear Er^{3+} tectons into 1D chains.
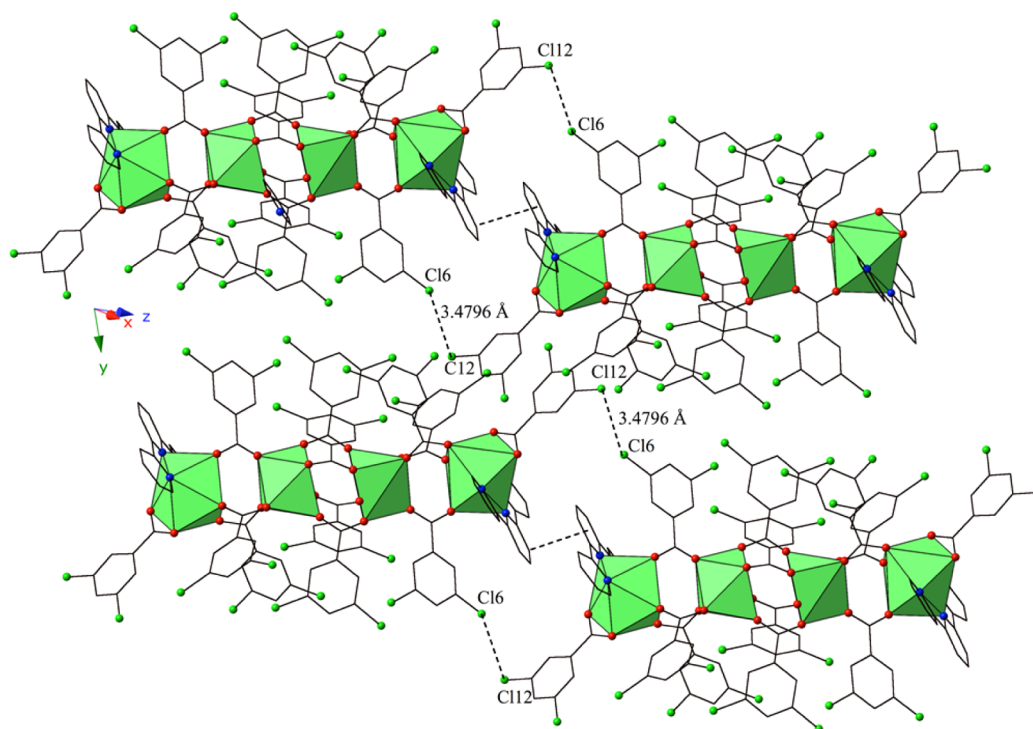
Figure 10. Complex **12** in approximately the (011) plane. Halogen–halogen and slightly offset π–π interactions, which assemble neighboring tectons of **12** into a supramolecular 2D sheet, are shown.

with slightly offset π–π interactions (Figure 10 and Figure S3). In **6**, assembly into 2D sheets results from four halogen–halogen interactions, yet in **12**, we observed only two unique Cl–Cl interactions. The halogen–halogen interactions are between

chlorines (Cl2, Cl6, Cl8, and Cl12) of 3,5-dichlorobenzoic ligands on neighboring units, whereas the slightly offset π–π interactions are between terpy ligands on different neighboring tectons. The two halogen–halogen interactions adopt geometries
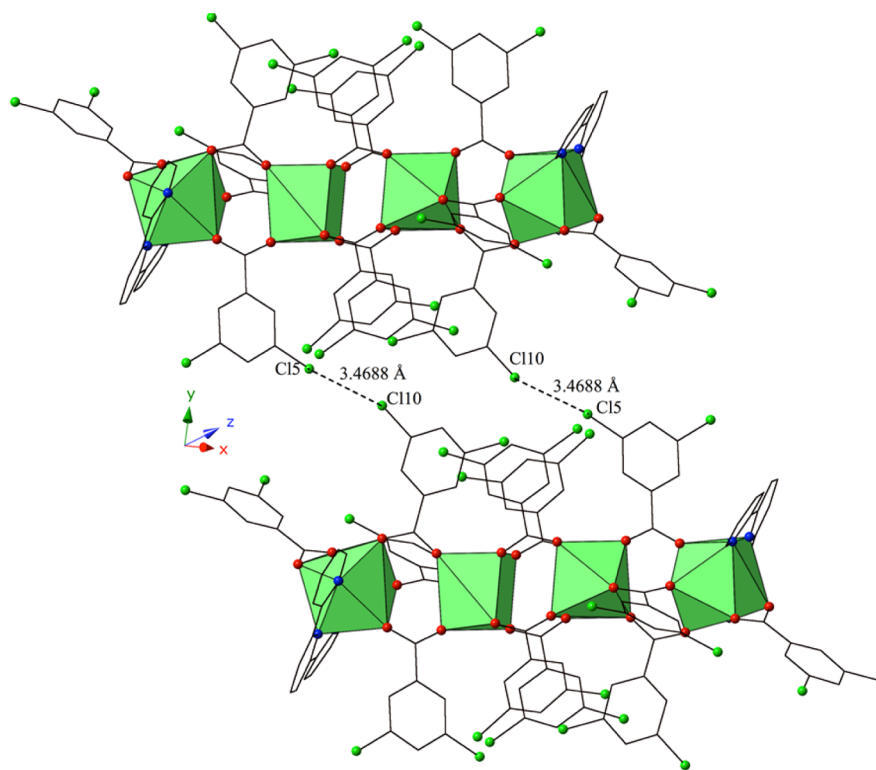
Figure 11. Complex **6** in approximately the (110) plane. The type I halogen–halogen interaction that links Sm^{3+} tetramers into supramolecular 3D networks is highlighted.

that can be described as type II and type I[38] and have lengths of 3.4796(12) Å (Cl6–Cl12) and 3.4022(12) Å (Cl2–Cl8), respectively (Figure 10 and Figure S3). Corresponding angles (∠C–Cl⋯Cl) for the interactions are 141.21(10)° and 100.43(9)° (type II Cl6–Cl12 interaction) and 136.77(11)° and 131.47(10)° (type I Cl2–Cl8 interaction). The offset π–π interactions[41] are between terpy ligands on adjacent tectons, and the methods for calculating centroid distances and angles have been defined previously.[23,42] The relevant distances and angles for these interactions in **12** are as follows: Cg⋯Cg, 3.5509(18) Å; Cg⊥⋯Cg⊥, 3.3442(12) Å; β, 19.64° (Figure 10).

Further assembly of the tectons of **12** to form a supramolecular 3D network is the result of a fourth unique halogen–halogen interaction along with a strong[40] localized Cl–π interaction (Figure 11 and Figure S4). Consistent with the halogen–halogen interactions described above, the interaction is once again between chlorines (Cl5 and Cl10) on 3,5-dichlorobenzoic acid ligands on neighboring tetrameric units. The interaction (Cl5–Cl10) adopts a geometry that can be described as type I[38] and has a length of 3.4688(14) Å with ∠C–Cl⋯Cl angles of 172.05(10)° and 159.63(11)° (Figure 11). Completing the assembly of the tetramers of **12** into a supramolecular 3D framework is a strong[40] localized Cl–π interaction (Cl4–C37) between 3,5-dichlorobenzoic acid ligands on adjoining units. The interactions between the chlorine (Cl4) of one 3,5-dichlorobenzoic acid and the periphery of the benzene ring of a 3,5-dichlorobenzoic acid ligand (C37) on the neighboring unit have a distance of 3.233(3) Å, (93.7% of the sum of the van der Waals radii), which is indicative of significant overlap between the two atoms (Figure S4).

Structural Discussion. Complexes **1–16** were each prepared under similar reaction conditions and thus provide a platform for

discussion of structure types in context with the effect of cation size on tecton nuclearity and subsequent means of noncovalent assembly. A goal of crystal engineering of hybrid materials is to control the assembly of metal-containing species, and recently, our group has begun to explore lanthanide hybrid materials in this regard.[22–24] This has been coupled with our ongoing work exploring halogen bonding in uranyl chemistry[26,42–44] and metal-ion hydrolysis in f-element systems.[6,45] Our initial efforts to explore halogen bonding in lanthanide hybrid materials,[22,23] and more specifically assembly via halogen–halogen interactions, yielded two families of monomers and dimers featuring the monofunctionalized *p*-chlorobenzoic acid ligand, which utilized a wide array of supramolecular synthons for assembly. With the goal of exercising greater control over assembly, we selected the 3,5-dichlorobenzoic acid ligand as it increased the number of chlorine sites at the periphery of the rare-earth tectons. 3,5-dichlorobenzoic acid has been used as a ligand in lanthanide coordination polymers[46] and as a linker molecule in Ln^{3+}–TM^{2+} bimetallic materials,[47] yet this appears to be the first instance in which it was selected for inclusion in Ln^{3+} hybrid materials explicitly for crystal engineering purposes and to provide a platform for comprehensively exploring supramolecular assembly as a function of RE^{3+} ionic radii.

In complexes **1–3** (structure types I and II), featuring either La^{3+} or Ce^{3+}, each Ln^{3+} metal center is bound to a tridentate terpy ligand and then further coordinated to three crystallographically unique 3,5-dichlorobenzoic acid ligands. In **1**, the 3,5-dichlorobenzoic acid ligands adopt μ_3-chelating–bridging and bidentate coordination modes and each La^{3+} metal center has a coordination number of 10. Looking at the modes of assembly of **1** reveals that the dimeric tectons are linked to a supramolecular 2D sheet via a type I halogen–halogen interaction along with a localized Cl–π interaction (Figure 2 and Table 3). PXRD analysis

Table 3. Structural Summary of Ln−3,5-Dichlorobenzoic Acid−2,2′:6′,2″-Terpyridine Materials (1−16)

	structure type I (La³⁺)	structure type II (La³⁺ and Ce³⁺)	structure type III (Pr³⁺−Tb³⁺)	structure type IV (Dy³⁺−Y³⁺)
tecton	dimer	dimer	tetramer	tetramer
Ln³⁺ coordination number(s)	10	9	8, 8	8, 7
supramolecular interactions (per tecton)	Cl−Cl, Cl−π	Cl−Cl (×2), Cl−π, Cl−O	Cl−Cl (×5), Cl−O	Cl−Cl (×4), Cl−π, Cl−O, π−π
dimensionality	2D	3D	3D	3D

reveals **1** is a minor phase with complex **2** (Figure S8), and in both **2** and Ce³⁺ analogue **3**, the benzoic acid ligands adopt three different coordination modes: monodentate, bidentate, and bridging bidentate. The coordination spheres of each Ln³⁺ cation also feature a bound water molecule to give each Ln³⁺ metal center a coordination number of 9. As highlighted in Figure 4 and Figure S1, the dimers of **2** and **3** are assembled into supramolecular 3D networks, an increase in dimensionality compared to that of **1**, and the assembly is now a result of a bifurcated halogen−halogen interaction along with localized Cl−π interactions and halogen bonding (Table 3).

In complexes **4−16** (structure types III and IV), from Pr³⁺ to Y³⁺, an increase in nuclearity is observed (compared to structure types I and II), and each tetramer features two unique RE³⁺ coordination environments. Structure type III (Pr³⁺−Tb³⁺) features two Ln³⁺ metal centers that are each eight-coordinate. Using complex **6** (Sm³⁺) as a reference, Sm1 is bound by eight carboxylate oxygen atoms, five from bridging bidentate 3,5-dichlorobenzoic ligands and three from a μ_3-chelating−bridging carboxylate, whereas Sm2 is chelated by a terpy moiety and bound to four 3,5-dichlorobenzoic acid ligands adopting two coordination modes (bridging bidentate and bidentate). The tetramers of **6** are assembled into a supramolecular 3D network, similar to structure type II, via five unique halogen−halogen interactions and a halogen bonding interaction. (Figures 6 and 7, Figure S2, and Table 3). Structure type IV (Dy³⁺−Y³⁺) is very similar to structure type III in terms of its local coordination environment with one change in carboxylate coordination, an evolution from a μ_3-chelating−bridging carboxylate to a bridging bidentate coordination mode (highlighted in Figure 8), likely a result of the decreasing ionic radii of the RE³⁺ metal centers. Looking at the modes of supramolecular assembly of complex **12**, we note that this small change in local coordination environment manifests as a change of the type of halogen bonding interaction observed. Whereas structure type III is assembled into a 3D network via halogen−halogen and halogen bonding interactions, structure type IV uses halogen−halogen, halogen bonding, halogen−π, and offset π−π interactions to link the tectons into a supramolecular 3D network. (Figures 9−11, Figures S3 and S4, and Table 3).

Luminescence. Solid-state photoluminescent spectra (room temperature) were obtained for complexes **6** (Sm³⁺), **7** (Eu³⁺), **9** (Tb³⁺), **10** (Dy³⁺), **12** (Er³⁺), and **14** (Yb³⁺). The photoluminescent behavior of **11** (Ho³⁺) and **13** (Tm³⁺) was also investigated in the near-IR and visible regions, respectively, yet the characteristic peaks of these two Ln³⁺ ions were not observed. Luminescence data for complexes **4** (Pr³⁺) and **5** (Nd³⁺) were not obtained as the bulk samples of these preparations were not phase pure (Figures S11 and S12). Complexes were excited at wavelengths corresponding to the absorption maxima of the terpy ligand, which functions to sensitize the Ln³⁺ centers in these materials.

For complexes **6** (Sm³⁺) and **7** (Eu³⁺), the characteristic $^4G_{5/2} \rightarrow {}^6H_J$ ($J = {}^5/_2 \rightarrow {}^9/_2$) and $^5D_0 \rightarrow {}^7F_J$ ($J = 0 \rightarrow 3$) transitions were observed at approximately 563, 598, and 644 nm (for **6**) and
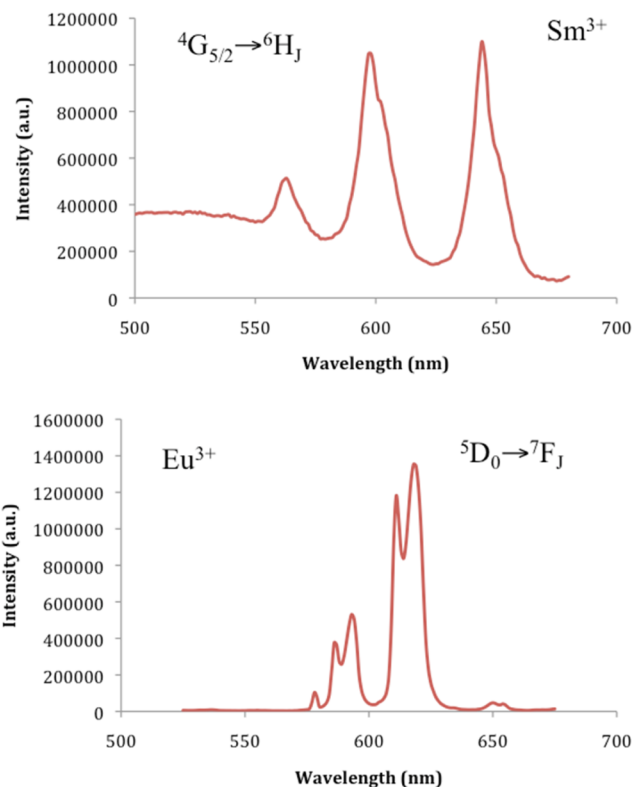

Figure 12. Solid-state emission spectrum for Sm³⁺ complex **6** (top) and solid-state emission spectrum for Eu³⁺ complex **7** (bottom).

578, 593, 618, and 650 nm (for **7**), respectively (after excitation at 348 nm) (Figure 12). The most intense of the three visible transitions for **6** is the hypersensitive $^4G_{5/2} \rightarrow {}^6H_{9/2}$ transition that, along with the $^4G_{5/2} \rightarrow {}^6H_{7/2}$ magnetic-dipole transition, is responsible for the red-orange color of Sm³⁺ emission.[48] For **7**, the spectrum is dominated by the hypersensitive $^5D_0 \rightarrow {}^7F_2$ transition at ∼618 nm, which is responsible for the characteristic red luminescence of Eu³⁺ materials. Additionally, the $^5D_0 \rightarrow {}^7F_2$ transition is significantly more intense than the $^5D_0 \rightarrow {}^7F_1$ magnetic-dipole transition, which coupled with the splitting observed in both of these transitions is consistent with crystallographic observations, which indicate that the Eu³⁺ metal centers of **7** are in low-symmetry environments.[49,50]

The four spectral bands of **9** (Tb³⁺) at 489, 542, 584, and 620 nm correspond to the $^5D_4 \rightarrow {}^7F_J$ ($J = 6 \rightarrow 3$) electronic transitions of the Tb³⁺ ion and were obtained using an excitation wavelength of 343 nm (Figure 13). The strongest observed transition was the $^5D_4 \rightarrow {}^7F_5$ band at ∼541 nm, which is responsible for the characteristic green color of Tb³⁺ emission.

The emission spectrum for complex **10** (Dy³⁺) reveals the expected Dy³⁺-centered peaks superimposed upon a residual fluorescence signal from the ligand components (Figure 14). The peaks at 477 and 570 nm can be assigned to the $^4F_{9/2} \rightarrow {}^4H_{15/2}$ and $^4F_{9/2} \rightarrow {}^4H_{13/2}$ transitions of Dy³⁺, respectively. The $^4F_{9/2} \rightarrow {}^4H_{13/2}$ electric-dipole transition of Dy³⁺ is often observed to be
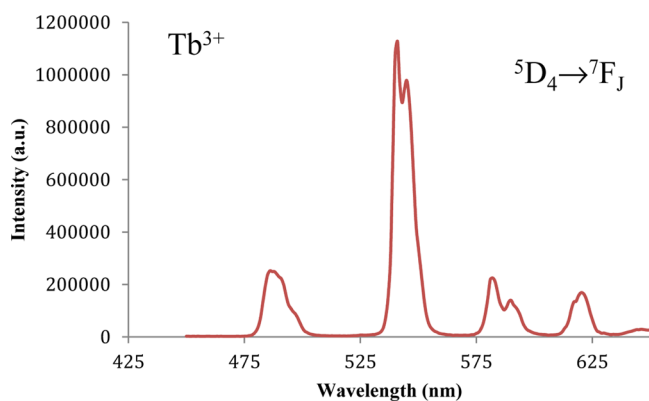
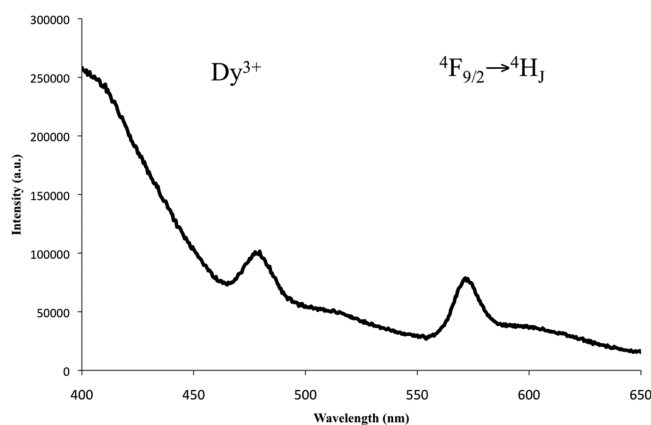**Figure 13.** Solid-state emission spectrum for Tb^{3+} complex **9**.

Figure 14. Solid-state emission spectrum for Dy^{3+} complex **10**.

the most intense, yet here the $^4F_{9/2} \rightarrow {}^4H_{15/2}$ magnetic-dipole transition is slightly more intense, suggesting that the terpy ligand is appropriate for the sensitization of the blue and yellow components of Dy^{3+} luminescence.[23,51,52]

The near-IR luminescence spectra of **12** (Er^{3+}) and **14** (Yb^{3+}) were collected after excitation at 355 nm and feature bands at 978 and 1521 nm corresponding to the characteristic $^2F_{5/2} \rightarrow {}^2F_{7/2}$ transition of Yb^{3+} and the $^4I_{13/2} \rightarrow {}^4I_{15/2}$ transition of Er^{3+}, respectively (Figure 15). A shoulder peak (~999 nm) in the
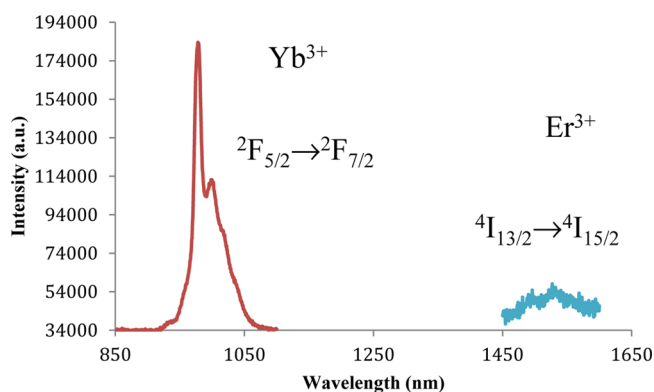

Figure 15. Solid-state emission spectra for Er^{3+} complex **12** and Yb^{3+} complex **14**.

spectrum of **14** is the likely result of unresolved M_J splitting of the emitting and/or fundamental states of Yb^{3+}, which may be induced by ligand field effects.

Whereas the room-temperature fluorescence spectrum of the Gd^{3+} complex (**8**) showed a dominant peak at 402 nm, low-temperature (77 K) measurements on the solid sample showed a red-shifted, weakly vibronically structured peak at 460−520 nm (upon excitation at 360 nm), with an approximated onset around 430 nm (23260 cm^{-1}) (Figures S5−S7). This energy value therefore suggests that sensitization of each of the emitting Ln^{3+} in the series is feasible via this state, assuming a sensitization mechanism that proceeds via the ligand-based triplet state.

Supporting time-resolved measurements were collected using a pulsed 355 nm light source and were obtained for complexes **6**, **7**, **9**−**12**, and **14** (Table 4). The data revealed that in the majority

Table 4. Visible and Near-IR Luminescence Lifetimes of Selected Ln−3,5-Dichlorobenzoic Acid−2,2′:6′,2″-Terpyridine Materials

complex	τ_{obs} (s)
6 (Sm^{3+})	2.02×10^{-6}
7 (Eu^{3+})	8.47×10^{-4}
9 (Tb^{3+})	6.77×10^{-4}
10 (Dy^{3+})	1.98×10^{-6}
11 (Ho^{3+})	$<25 \times 10^{-9}$
12 (Er^{3+})	2.55×10^{-6}
14 (Yb^{3+})	2.24×10^{-5}

of cases lifetime profiles were satisfactorily fitted to single-exponential decays. The magnitudes of lifetime values are broadly in line with the variations that are typically observed for luminescent species across the lanthanide series, with **7** (Eu^{3+}) and **9** (Tb^{3+}) displaying the longest lifetimes.

Magnetism. Direct current (dc) magnetic measurements were performed on complexes **10** and **12** between 1.8 and 300 K, with an applied dc field of 1000 Oe. The temperature dependence of the χT product for all samples can be observed in Figure 16. At room temperature, the observed χT values
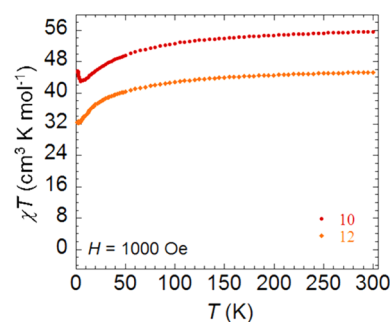

Figure 16. Temperature dependence of the χT product at 1000 Oe for **10** (Dy^{3+}) and **12** (Er^{3+}).

are as follows: 55.58 cm^3 K mol^{-1} for **10** and 45.16 cm^3 K mol^{-1} for **12**. The χT value for **10** is slightly lower than the theoretical value of 56.68 cm^3 K mol^{-1} for four noninteracting Dy^{3+} ions ($^6H_{15/2}$; $S = {}^5/_2$, $L = 5$, $g = {}^4/_3$, and $\chi T = 14.17$ cm^3 K mol^{-1}), and similarly, the χT value for **12** is also slightly lower than the theoretical value of 45.92 cm^3 K mol^{-1} for four non-interacting Er^{3+} ions ($^4I_{15/2}$; $S = {}^3/_2$, $L = 6$, $g = {}^6/_5$, and $\chi T = 11.48$ cm^3 K mol^{-1}). For both **10** and **12**, the χT product displays a gradual monotonous decrease in temperature until approximately 50 K, at which point a more dramatic drop is observed with χT values reaching 41.41 cm^3 K mol^{-1} at 4.5 K for **10** and 27.35 cm^3 K mol^{-1} at 3 K for **12**, before finally
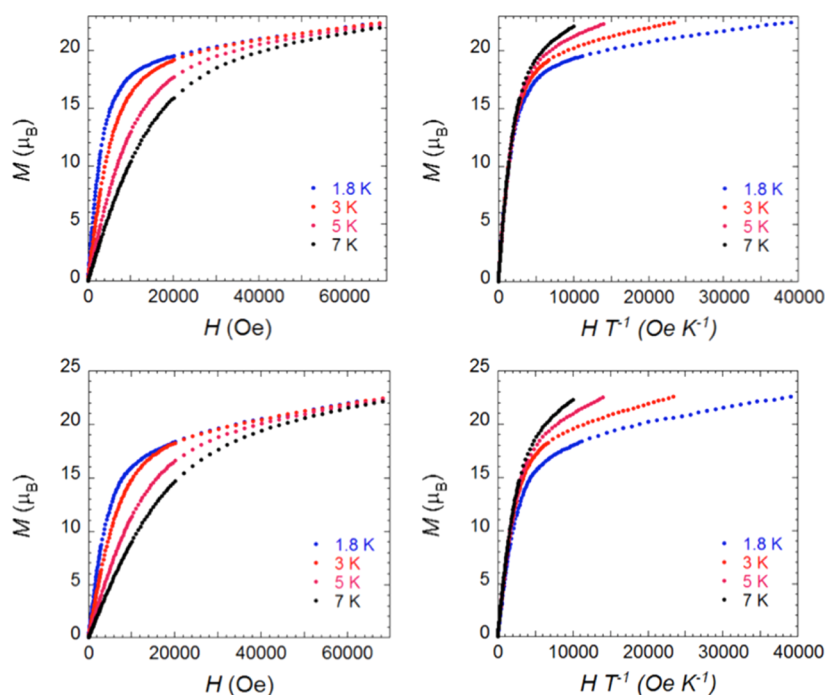
Figure 17. Field dependence (top) of the magnetization (left) and M vs HT^{-1} plot (right) of **10** (Dy^{3+}) at the indicated temperatures. Field dependence (bottom) of the magnetization (left) and M vs HT^{-1} plot (right) of **12** (Er^{3+}) at the indicated temperatures.

exhibiting a slight increase to 43.95 and 27.40 cm³ K mol⁻¹ at 1.8 K for **10** and **12**, respectively. This low-temperature increase in the χT product for both complexes is indicative of the presence of dominant ferromagnetic interactions between spin carriers. This type of low-temperature ferromagnetic interaction has been previously observed for Dy^{3+} binuclear complexes.[17,53,54] Because of the close contacts between spin carriers with the intramolecular unit of **10** [Dy1−Dy1, 4.2733(6) Å; Dy1−Dy2, 4.9549(7) Å] and **12** [Er1−Er1, 4.2587(7) Å; Er1−Er2, 4.9468(8) Å], as compared with the intermolecular closest distances of 9.310(1) and 16.314(2) Å for **10** and **12**, respectively, it is likely that intramolecular ferromagnetic interactions are taking place at very low temperatures. The consistent negative deviation of the χT product is most likely attributed to a combination of possible factors, such as inherent magnetic anisotropy present in Dy^{3+} and Er^{3+}, antiferromagnetic intramolecular interactions, and/or depopulation of the M_J states.

To confirm the presence of magnetic anisotropy, isotherm magnetization data were also collected between 1.8 and 7 K (Figure 17). In each complex, the M versus H data below 7 K demonstrate a rapid increase in the magnetization at low magnetic fields. A shoulder develops below 1 T, followed by a gradual increase in M at 1.8 K reaching 21.62 μ_B (**10**) and 19.00 μ_B (**12**) at 7 T without magnetic saturation. The M versus H/T data also display similar behavior for both complexes, where at high fields there is no saturation or overlay onto a single master curve. These properties indicate the presence of non-negligible magnetic anisotropy and/or low-lying excited states as is often observed in the late Ln^{3+} ions.

As a result of the observed magnetic anisotropy within **10** and **12**, we probed the dynamic magnetic behavior with ac susceptibility measurements. We observed the presence of a frequency-dependent increase in the in-phase susceptibility signal, along with the appearance of low-frequency tails in the out-of-phase susceptibility, under a small applied dc field, indicating the onset of field-induced slow relaxation of the magnetization. We were not

able to resolve the peaks to fit them to a generalized Debye model; thus, the relaxation processes of spin carriers within **10** and **12** are occurring too quickly for the instrument, likely because of the significant quantum tunneling of the magnetization (QTM), and/or other fast thermal relaxation processes, and we therefore cannot confirm the presence of SMM behavior within these complexes.

■ CONCLUSIONS

The preparation and crystal structures of 16 molecular rare-earth complexes featuring 3,5-dichlorobenzoic acid and 2,2′:6′,2″-terpyridine are reported. The types and frequency of supramolecular interactions within these materials have been analyzed, and the visible and near-IR luminescence spectra and radiative lifetimes (where possible) have been discussed. Further, the magnetic features of the tetranuclear Dy^{3+} (**10**) and Er^{3+} (**12**) complexes of the series were evaluated and displayed ferromagnetic behavior. The lanthanide contraction may be correlated to the structural changes and subsequent variation in types of supramolecular assembly motifs observed in structure types I−IV as one moves across the RE^{3+} series from La^{3+} to Y^{3+}. A closer look at the modes of supramolecular assembly in structure types I−IV suggests that one way to promote halogen bonding as a means of assembly in molecular rare-earth hybrids is simply to increase the number of halogen atoms at the periphery of the molecule, especially on a larger tecton, that results from RE^{3+} oligomerization. Follow-up studies focusing on probing interaction strength via infrared spectroscopy and focusing on shifts in C−X stretching frequencies as well as more detailed spectroscopic studies (i.e., solid-state quantum yields) are ongoing. Further, exploratory studies of supramolecular assembly and spectroscopic properties of molecular Ln^{3+} bimetallic materials are in progress.

■ ASSOCIATED CONTENT

ⓢ Supporting Information

The Supporting Information is available free of charge on the ACS Publications website at DOI: 10.1021/acs.inorgchem.6b00408.

CIFs have also been deposited at the Cambridge Crystallographic Database Centre and may be obtained from http://www.ccdc.cam.ac.uk by citing reference numbers 1453003−1453018 for compounds **1**-**16**, respectively.

> ORTEP figures of all compounds, PXRD patterns of all compounds, and tables of selected supramolecular interaction distances and bond lengths (PDF)
> X-ray crystallographic files (CIF)

■ **AUTHOR INFORMATION**

Corresponding Author

*E-mail: cahill@gwu.edu. Phone: (202) 994-6959.

Notes

The authors declare no competing financial interest.

■ **REFERENCES**

(1) Bünzli, J.-C. G.; Piguet, C. *Chem. Rev.* **2002**, *102*, 1897−1928.
(2) Bünzli, J.-C. G.; Piguet, C. *Chem. Soc. Rev.* **2005**, *34*, 1048−1077.
(3) Nief, F. In *Handbook on the Physics and Chemistry of Rare Earths*; Gschneidner, K. A., Bünzli, J.-C. G., Pecharsky, V. K., Eds.; Elsevier: Amsterdam, 2010; Vol. *40*, pp 241−300.
(4) Bradberry, S. J.; Savyasachi, A. J.; Martinez-Calvo, M.; Gunnlaugsson, T. *Coord. Chem. Rev.* **2014**, *273−274*, 226−241.
(5) de Bettencourt-Dias, A.; Barber, P. S.; Viswanathan, S. *Coord. Chem. Rev.* **2014**, *273−274*, 165−200.
(6) Carter, K. P.; Cahill, C. L. In *Handbook on the Physics and Chemistry of Rare Earths*; Bünzli, J.-C. G., Pecharsky, V. K., Eds.; Elsevier: Amsterdam, 2015; Vol. *47*, p 147−208.
(7) Barry, D. E.; Caffrey, D. F.; Gunnlaugsson, T. *Chem. Soc. Rev.* **2016**, *45*, 3244−3274.
(8) Bünzli, J.-C. G. *Chem. Lett.* **2009**, *38*, 104−109.
(9) Reddy, M. L. P.; Divya, V.; Pavithran, R. *Dalton Transactions* **2013**, *42*, 15249−15262.
(10) Martín-Ramos, P.; Coya, C.; Álvarez, Á. L.; Ramos Silva, M.; Zaldo, C.; Paixão, J. A.; Chamorro-Posada, P.; Martín-Gil, J. *J. Phys. Chem. C* **2013**, *117*, 10020−10030.
(11) Lima, P. P.; Paz, F. A. A.; Brites, C. D. S.; Quirino, W. G.; Legnani, C.; Costa e Silva, M.; Ferreira, R. A. S.; Júnior, S. A.; Malta, O. L.; Cremona, M.; Carlos, L. D. *Org. Electron.* **2014**, *15*, 798−808.
(12) Tancrez, N.; Feuvrie, C.; Ledoux, I.; Zyss, J.; Toupet, L.; Le Bozec, H.; Maury, O. *J. Am. Chem. Soc.* **2005**, *127*, 13474−13475.
(13) Law, G.-L.; Wong, K.-L.; Lau, K.-K.; Lap, S.-T.; Tanner, P. A.; Kuo, F.; Wong, W.-T. *J. Mater. Chem.* **2010**, *20*, 4074−4079.
(14) Luzon, J.; Sessoli, R. *Dalton Transactions* **2012**, *41*, 13556−13567.
(15) Woodruff, D. N.; Winpenny, R. E. P.; Layfield, R. A. *Chem. Rev.* **2013**, *113*, 5110−5148.
(16) Habib, F.; Murugesu, M. *Chem. Soc. Rev.* **2013**, *42*, 3278−3288.
(17) Hutchings, A.-J.; Habib, F.; Holmberg, R. J.; Korobkov, I.; Murugesu, M. *Inorg. Chem.* **2014**, *53*, 2102−2112.
(18) Bünzli, J.-C. G. *J. Coord. Chem.* **2014**, *67*, 3706−3733.
(19) Meyer, L. V.; Schonfeld, F.; Müller-Buschbaum, K. *Chem. Commun.* **2014**, *50*, 8093−8108.
(20) Cucinotta, G.; Perfetti, M.; Luzon, J.; Etienne, M.; Car, P.-E.; Caneschi, A.; Calvez, G.; Bernot, K.; Sessoli, R. *Angew. Chem., Int. Ed.* **2012**, *51*, 1606−1610.
(21) Silva, M. R.; Martin-Ramos, P.; Coutinho, J. T.; Pereira, L. C. J.; Martin-Gil, J. *Dalton Transactions* **2014**, *43*, 6752−6761.

(22) Carter, K. P.; Pope, S. J. A.; Cahill, C. L. *CrystEngComm* **2014**, *16*, 1873−1884.
(23) Carter, K. P.; Zulato, C. H. F.; Cahill, C. L. *CrystEngComm* **2014**, *16*, 10189.
(24) Carter, K. P.; Zulato, C. H. F.; Rodrigues, E. M.; Pope, S. J. A.; Sigoli, F. A.; Cahill, C. L. *Dalton Transactions* **2015**, *44*, 15843−15854.
(25) Constable, E. C. *Chem. Soc. Rev.* **2007**, *36*, 246−253.
(26) Carter, K. P.; Cahill, C. L. *Inorg. Chem. Front.* **2015**, *2*, 141−156.
(27) Carter, K. P.; Kalaj, M.; Cahill, C. L. *Eur. J. Inorg. Chem.* **2016**, *2016*, 126−137.
(28) *SAINT*; Bruker AXS Inc.: Madison, WI, 2007.
(29) *APEX2*; Bruker AXS Inc.: Madison, WI, 2008.
(30) Krause, L.; Herbst-Irmer, R.; Sheldrick, G. M.; Stalke, D. *J. Appl. Crystallogr.* **2015**, *48*, 3−10.
(31) *TWINABS*; Bruker AXS Inc.: Madison, WI, 2008.
(32) Altomare, A.; Cascarano, G.; Giacovazzo, C.; Guagliardi, A.; Burla, M. C.; Polidori, G.; Camalli, M. *J. Appl. Crystallogr.* **1994**, *27*, 435.
(33) Sheldrick, G. *Acta Crystallogr., Sect. A: Found. Crystallogr.* **2008**, *64*, 112−122.
(34) Farrugia, L. *J. Appl. Crystallogr.* **2012**, *45*, 849−854.
(35) *Crystal Maker*; Crystal Maker Software Limited: Bicester, England, 2009.
(36) *JADE*; Materials Data Inc.: Livermore, CA, 2003.
(37) Desiraju, G. R.; Parthasarathy, R. *J. Am. Chem. Soc.* **1989**, *111*, 8725−8726.
(38) Mukherjee, A.; Tothadi, S.; Desiraju, G. R. *Acc. Chem. Res.* **2014**, *47*, 2514−2524.
(39) Schollmeyer, D.; Shishkin, O. V.; Ruhl, T.; Vysotsky, M. O. *CrystEngComm* **2008**, *10*, 715−723.
(40) Mooibroek, T. J.; Gamez, P.; Reedijk, J. *CrystEngComm* **2008**, *10*, 1501−1515.
(41) Janiak, C. *J. Chem. Soc., Dalton Trans.* **2000**, 3885−3896.
(42) Surbella, R. G., III; Cahill, C. L. *CrystEngComm* **2014**, *16*, 2352−2364.
(43) Deifel, N. P.; Cahill, C. L. *Chem. Commun.* **2011**, *47*, 6114−6116.
(44) Andrews, M. B.; Cahill, C. L. *Dalton Transactions* **2012**, *41*, 3911−3914.
(45) Andrews, M. B.; Cahill, C. L. *Chem. Rev.* **2013**, *113*, 1121−1136.
(46) Tan, X.; Che, Y.-X.; Zheng, J.-M. *Inorg. Chem. Commun.* **2013**, *35*, 231−234.
(47) Zhao, F.-H.; Li, H.; Che, Y.-X.; Zheng, J.-M.; Vieru, V.; Chibotaru, L. F.; Grandjean, F.; Long, G. J. *Inorg. Chem.* **2014**, *53*, 9785−9799.
(48) Biju, S.; Eom, Y. K.; Bünzli, J.-C. G.; Kim, H. K. *J. Mater. Chem. C* **2013**, *1*, 6935−6944.
(49) Rodrigues, M. O.; da Costa Junior, N. B.; de Simone, C. A.; Araujo, A. A. S.; Brito-Silva, A. M.; Paz, F. A. A.; de Mesquita, M. E.; Junior, S. A.; Freire, R. O. *J. Phys. Chem. B* **2008**, *112*, 4204−4212.
(50) Shavaleev, N. M.; Scopelliti, R.; Gumy, F.; Bünzli, J.-C. G. *Inorg. Chem.* **2009**, *48*, 6178−6191.
(51) Xu, J.; Cheng, J.; Su, W.; Hong, M. *Cryst. Growth Des.* **2011**, *11*, 2294−2301.
(52) Ahmed, Z.; Iftikhar, K. *J. Phys. Chem. A* **2013**, *117*, 11183−11201.
(53) Pointillart, F.; Golhen, S.; Cador, O.; Ouahab, L. *Eur. J. Inorg. Chem.* **2014**, *2014*, 4558−4563.
(54) Moreno Pineda, E.; Chilton, N. F.; Marx, R.; Dörfel, M.; Sells, D. O.; Neugebauer, P.; Jiang, S.-D.; Collison, D.; van Slageren, J.; McInnes, E. J. L.; Winpenny, R. E. P. *Nat. Commun.* **2014**, *5*, 5243−5249.